AN APPLICATION OF THE SCALED–PIXEL–COUNTING PROTOCOL
TO QUANTIFY THE RADIOLOGICAL FEATURES OF ANATOMICAL STRUCTURES
OF THE NORMAL TARSAL JOINT IN HORSES

Marta BOROWSKA*, **Bernard TUREK****, **Paweł LIPOWICZ***, **Tomasz JASIŃSKI****,
Katarzyna SKIERBISZEWSKA**, **Małgorzata DOMINO****

*Institute of Biomedical Engineering, Faculty of Mechanical Engineering, Bialystok University of Technology,
ul. Wiejska 45C, 15-351 Bialystok, Poland
**Department of Large Animal Diseases and Clinic, Institute of Veterinary Medicine, Warsaw University of Life Sciences,
ul. Nowoursynowska 166, 02-787 Warsaw, Poland

m.borowska@pb.edu.pl, bernard_turek@sggw.edu.pl, p.lipowicz@pb.edu.pl, jasinski_tomasz@sggw.edu.pl,
katarzyna_skierbiszewska@sggw.edu.pl, malgorzata_domino@sggw.edu.pl

Abstract: Background: As high-performance human and equine athletes train and compete at the highest level of effort, the prevention of high-performance-cased diseases, such as osteoarthritis (OA), requires knowledge of the anatomy and physiology of the subjected bones. Objective: Implementation of the scaled–pixel–counting protocol to quantify the radiological features of anatomical structures of the normal equine tarsal joint as the first step in the prevention of the tarsal joints OA in high-performance sport horses. Methods: A radiographic examination was performed in six cadaverous equine pelvic limbs. The dorso–plantar projection of the tarsal joint was performed using density standard (DS) attached to the radiographic cassette, standard X-ray equipment and standard diagnostic imaging protocol. On each of the radiographs, pixel brightness (PB) was extracted for each of the 10 steps (S1–S10) of DS. On each of the radiographs, seven regions of interest (ROIs) were annotated representing four bones (II tarsal bone [II TB], III tarsal bone [III TB], IV tarsal bone [IV TB] and central tarsal bone [CTB]) and three joints (proximal intertarsal joint [PIJ], distal intertarsal joint [DIJ] and tarsometatarsal joint [TMJ]), respectively. For each ROI, the percentage (%) of number of pixels (NP) from each range was calculated. Results: The % of NP was lower in bones than in joint spaces for S1–S6 and was higher in bones than in joint spaces for S8–S10. The % of NP was higher in PIJ than TMJ for S1 and higher in PIJ than DIJ for S4. No differences were found between consecutive bones for all examined steps of DS. Conclusions: An application of the scaled–pixel–counting protocol provides the quantitative radiological features of normal bone and joint structures of the tarsal joint in horses, making possible differentiation of the lucency of joint space and opacity of bone structure.

Key words: diagnostic imaging, radiographs, radiodensity, osteoarthritis, prevention, horse

1. BACKGROUND

Nowadays, the sport uses of horses in show jumping, eventing, dressage, driving, reining, vaulting or endurance are characterised by the horse being perceived as an athlete in its own right [1]. In high-performance sports, both human and equine athletes train and compete at the highest level of effort. However, one should keep in mind that the level is close to the limit of injury, as exceeding their physiological limits allows for the achievement of the best performance results [2]. The powerhouse of athletic movement is the muscle [3], whereas the skeletal system withstands the stressors placed on bones and joints during high-performance exercises [2]. Therefore, the cultivation of a deep knowledge of the anatomy and physiology of the equine skeletal system is the first step in the prevention of high-performance-cased diseases.

One of the important causes of lameness, and thus the exclusion of a sport horse from high-performance, is osteoarthritis (OA) [4]. OA is a joint disease that results from joint cartilage and underlying bone destruction. Cartilage destruction and subchondral bone sclerosis are central and irreversible steps in OA, although the entire joint is affected [2]. As OA occurs more commonly in the overload joint, repeated stress on bones and ligaments has been suggested to be important in the development of OA. Show jumping horses are often affected by the metacarpophalangeal joint OA due to forces acting during landing after a jump, whereas dressage and reining horses often suffer from the tarsal joints OA due to strong involvement of the hindquarters during exercise [5]. The OA is diagnosed based on the clinical symptoms such as lameness and stiffness, which in many cases reduce the working capacity of the horse [6–8]. The clinical symptoms are relevant to the low-grade chronic inflammation typical for OA. Therefore, the diagnostic strategy considers the basic clinical examination and the detailed orthopaedic examination supported by the flexion tests, response to local anaesthesia and diagnostic imaging of the affected joint [6, 7]. While radiographic changes in the tarsal joint have variable correlation with lameness [6, 8–10], radiographs are frequently used to identify structural changes in the clinically suspected joint [6]. Within the structural changes identified by radiographs in affected joints, joint space narrowing, lysis of subchondral bone, sclerosis of subchondral bone, mineralisation front defects and osteophyte/enthesophyte development should be considered [6, 7, 10, 11].

One of the equine limb joints most commonly diagnosed with OA is the tarsal joint. In the experience from clinical cases, there

is evidence indicating that the OA in the tarsal joint is a slowly progressing disease where clinical symptoms may precede radiographic signs of degenerative joint disease [8]. Spontaneous radiographic signs of OA in the tarsal joint have been reported in 30%–60% of the horse population, with a higher prevalence in mature horses [6, 8–10]. The OA in the tarsal joint has been suggested to be most frequent in older horses. Type and load of work, limb conformation and developmental abnormalities have been proposed as factors predisposing to the OA in the tarsal joint [8]. The OA in the distal intertarsal joint (DIJ), tarsometatarsal joint (TMJ) and less proximal intertarsal joint (PIJ) occurs commonly in sport horses; thus, structural changes' identification may help in OA prognosis determination and the monitoring of disease [7, 10, 11]. The onset of the OA in the tarsal joint is often followed by a period during which degenerative changes worsen and clinical symptoms of varying degrees are present continuously or intermittently. However, the progression of the disease as evaluated by radiological examination remains to be investigated as not all individuals reach the final stage of ankylosis [8]. The monitoring of the radiographic signs is particularly important when the outcome of both spontaneous ankylosis [8] and surgical arthrodesis [12, 13] of tarsal joints is assessed.

One may observe that OA structural changes are quantified using the radiographic rating systems, which are commonly used in humans [14, 15], occasionally used in dogs [16] and increasingly used in equines [12, 13]. These systems attempt to assign an aggregate score based on the appearance and severity of recognised disease features [12–17]. Besides the adaptation of the Delphi technique that considers the expert consultation process [18], none of the developed rating systems allow radiographic signs grading in detail for each tarsal bone (TB) and joint independently, and therefore none of the existing radiographic rating systems is unlikely to be useful in the clinic [18]. Labens et al. [18] concluded that they do not advocate the clinical use of the radiographic rating scale developed in the recent literature unless each user assesses his repeatability first. Moreover, they concluded that the knowledge of radiographic features selected by the experts according to their diagnostic value for the tarsal joint OA may be of considerable importance to the development of other rating scales. They suggested that the new rating systems may include a scale based on the recognition of the selected radiographic features and the assignment of a numeric value. To fill the gap in the existing state of quantification of the radiological signs of the tarsal joint OA, the objective of this study is to implement the scaled–pixel–counting protocol to quantify the radiological features of the anatomical structures of the equine normal tarsal joint as the first step in the prevention of the tarsal joints OA in the high-performance sport horses.

2. METHODS

The study was conducted on six cadaverous equine pelvic limbs with no clinical symptoms and radiological signs of the tarsal joint OA. Limbs were collected during post-mortem at the commercial slaughterhouse in Poland, which does not fall under the legislation for the protection of animals used for scientific purposes, national decree-law (Dz. U. 2015 poz. 266) and the European Union law (2010-63-EU directive). Thus, no Ethical Committee's permission was needed for sample retrieval after slaughter. The absence of clinical symptoms of OA was determined as the initial

inclusion criterion; thus, the orthopaedic examination, limited to slaughter specimen, was performed considering swelling, joint deformities and impaired function of the affected joint manifested by decreased motion range. The orthopaedic examination was performed by palpation in lateral and anterior-posterior recumbency. During the orthopaedic examination, the lack (0) or presence (1) of swelling, joint deformities and decreased motion range was noted. The initial exclusion criterion was the presence of at least one clinical symptom of tarsal joint OA. Based on the initial exclusion criterion, no limb was excluded.

Then, the radiographic examination of the tarsal joint was performed using an X-ray tube (Orange 9020HF, Ecoray Co., Seoul, South Korea), a radiographic cassette (Saturn 8000, Vievorks Co., Seoul, South Korea) and a portable computer (HP Inc. UK Ltd., Reading, UK). The X-ray tube settings were 1.25 mAs and 60 kV, and the distance between the X-ray tube and radiographic cassette was 80 cm (Fig. 1A). The density standard (DS) was attached to the radiographic cassette while each radiograph was taken. The DS was positioned perpendicular to the surface of the cassette so that the long axis of the DS was parallel to the long axis and the thick end was caudally of the cassette (Fig. 1B, C). Concomitant with the cassette and DS being subject to such preparation, the dorso–plantar projection of the tarsal joint, with the centre of the X-ray beam positioned on the central tarsal bone (CTB), was performed. As Labens et al. [18] did not find significant differences between the equine tarsal joint ratings for each radiographic projection, considering the lateromedial view, dorso–plantar view and planto–dorsal view, the only one dorso–plantar projection of the tarsal joint in the current preliminary study was used. The radiographs were acquired as .jpg files.
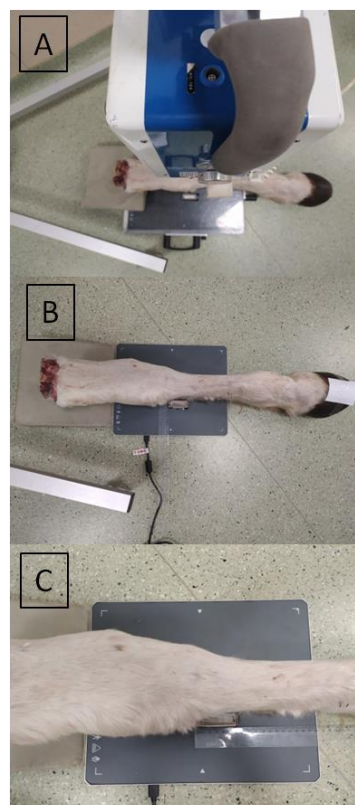
Fig. 1. The position of the X-ray tube on a tripod in relation to the cadaverous pelvic limb and radiographic cassette (A). The position of the density standard (DS) in relation to the long (B) and short (C) edges of the radiographic cassette
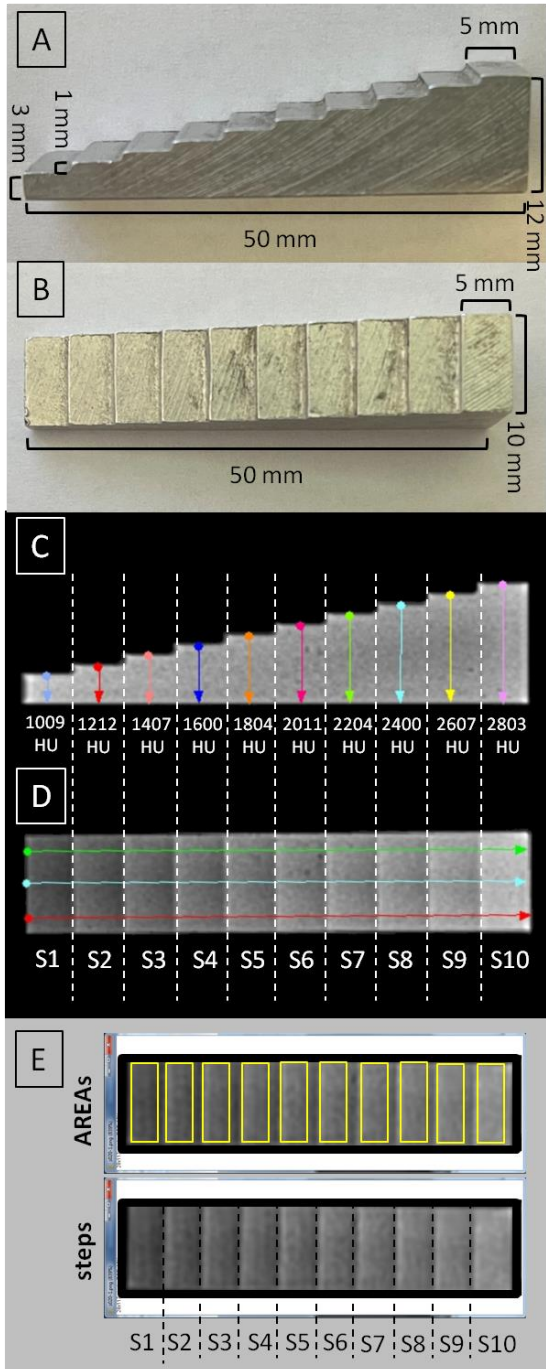
Fig. 2. The density standard (DS) in visible light (A, B) and under X-ray beam (C, D, E) – side view (A, C) and top view (B, D, E). Views concerning 10 steps (S1–S10) of an irregular cuboid. Views with marked dimensions (A, B), attenuation of the X-ray beam (C, D) and rectangular regions of interest representing S1–S10 (AREAs) (E)

Each radiograph was visually assessed for the presence of radiological signs of the tarsal joint OA. The absence of radiological signs of OA was determined as the secondary inclusion criterion; thus, the radiograms evaluation considered joint space narrowing, lysis of subchondral bone, sclerosis of subchondral bone, mineralisation front defects and osteophyte/enthesophyte [6, 7, 10, 11]. The radiograph evaluation was visually assessed. The lack (0) or presence (1) of radiological signs of joint space narrowing, lysis of subchondral bone, sclerosis of subchondral bone,

mineralisation front defects and osteophyte/enthesophyte was noted. The secondary exclusion criterion was the presence of at least one radiological sign of tarsal joint OA. Based on the secondary exclusion criterion, no limb was excluded.

The DS is an irregular cuboid with 10 steps (S1–S10) made of aluminium (Al; 95.20–98.88 Mass%; 92.71–98.92 Atom%). The DS dimensions are 55 mm in length on the basis, 12 mm high in the highest place, 3 mm high in the lowest place and 10 mm wide (Fig. 2A, B). The attenuation of the X-ray beam passing through the DS was reported in the form of the Hounsfield unit (HU) measured for each of S1–S10 as follows: S1 = 1009 HU, S2 = 1212 HU, S3 = 1407 HU, S4 = 1600 HU, S5 = 1804 HU, S6 = 2011HU, S7 = 2204 HU, S8 = 2400 HU, S9 = 2607 HU and S10 = 2803 HU (Fig. 2C, D).

On each radiograph (Fig. 3A), seven polymorphic regions of interest (ROIs) were manually annotated using ImageJ software (version 1.46r, Wayne Rasband, Bethesda, MD, USA). ROIs represented seven anatomical structures of the normal tarsal joint including four bones (II tarsal bone [II TB], III tarsal bone [III TB], IV tarsal bone [IV TB] and central tarsal bone [CTB]) (Fig. 3B–E) and three joints (proximal intertarsal joint [PIJ], distal intertarsal joint [DIJ] and tarsometatarsal joint [TMJ]) (Fig. 3F–H).
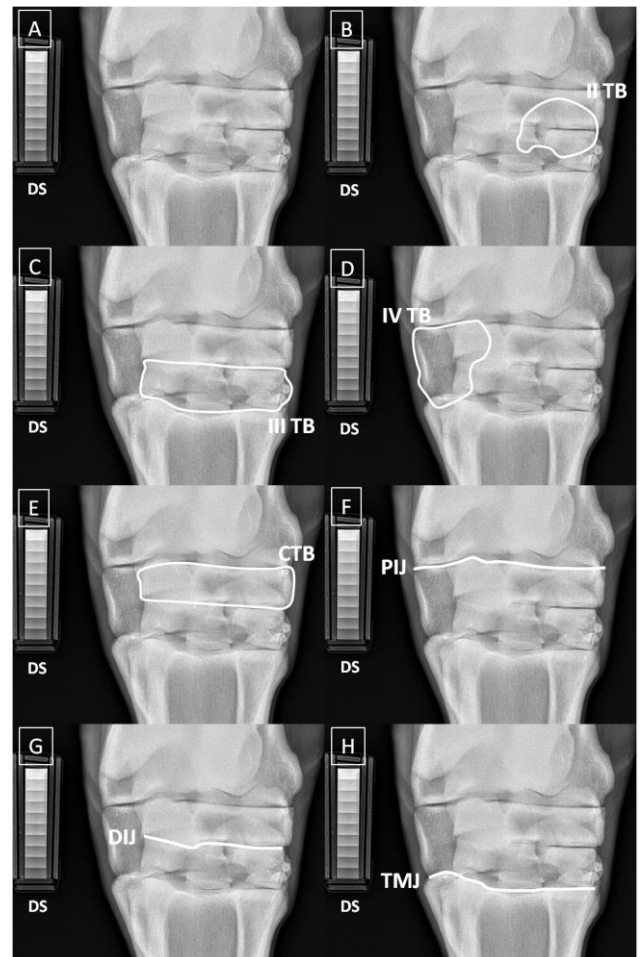
Fig. 3. The radiograph of the normal tarsal joint in horses without (A) and with (B–H) annotated regions of interest (ROIs). ROIs represented II tarsal bone (II TB) (B), III tarsal bone (III TB) (C), IV tarsal bone (IV TB) (D), central tarsal bone (CTB) (E), proximal intertarsal joint (PIJ) (F), distal intertarsal joint (DIJ) (G) and tarsometatarsal joint (TMJ) (H). The density standard (DS) is visible in each image

Additionally, 10 rectangular regions of interest representing S1–S10 (AREAs) were manually annotated using ImageJ software (Fig. 2E). The AREAs represented 10 steps of DS with various degrees of X-ray beam attenuation. Each AREAs returned the values of Pixel Brightness (PB) <0; 255> and determined the ranges of PB change in each AREAs. AREAs that attenuated a small amount of the X-ray beam (e.g. soft tissues) were dark and represented an area of lucency. AREAs that attenuate a large amount of the X-ray beam (e.g. bones) were bright and represented an area of opacity. The algorithm of the scaled pixel counting protocol was implemented in Python:

```
M = image*mask
start = 1
for i in range(R):
    if i=R-1: end = PBMax
    else: end = AREA[i]+(Area[i+1] AR-
EA[i])/2)
    NP = len(M[(M>=start)&(M<=end)])
    %NP =
    start = end+1
```

where the notations are as follows:
- M – segmented image
- image – input image
- mask – mask image
- start – beginning of the interval
- end – ending of the interval
- R – number of S-labelled data series
- Area – vector of intervals S-labelled data series
- NP – pixel counting result
- % NP – normalisation of NP
  The features of the algorithm are:
- the algorithm is designed for grayscale images;
- the result depends on the image intensity of the ROIs;
- in each image, AREAs were annotated to compare the beam attenuation of individual ROIs; and
- the result is independent of artefacts generated during registration, and thus each measurement is independent.

The number of pixels (NP) values was grouped for all bone's and joint's anatomical structures, assigned to 10 S-labelled data series (S1, S2, S3, S4, S5, S6, S7, S8, S9 and S10) and tested independently for univariate distributions using the Kolmogorov–Smirnov normality test. The S-labelled NP data series were compared between all bone's and joint's anatomical structures, using the Mann–Whitney test. The NP values were grouped for the consecutive bone's and joint's anatomical structures, assigned to 10 S-labelled data series and tested independently for univariate distributions using the Kolmogorov–Smirnov normality test. The S-labelled NP data series were compared between bone's (II TB vs III TB vs IV TB vs CTB) and joint's (PIJ vs DIJvs TMJ) anatomical structures separately, using the Kruskal–Wallis test followed by the Dunn's multiple comparisons test. For each data set, at least one data series was non-Gaussian distributed. The alpha value was established as α = 0.05. All statistical analyses were performed using Graph Pad Prism 6 software (GraphPad Software Inc., Avenida De La Playa La Jolla, CA, USA).

3. RESULTS

The % of NP was lower in bones than in joint spaces for S1 (Fig. 4A), S2, (Fig. 4B), S3 (Fig. 4C), S4 (Fig. 4D), S5 (Fig. 4E) and S6 (Fig. 4F), which made it possible to indicate the lucency of joint space. Moreover, the % of NP was higher in bones than in joint spaces for S8 (Fig. 4H), S9 (Fig. 4I) and S10 (Fig. 4J), which made it possible to indicate the opacity of bone structure. No difference was found between bones and joints for S7 (Fig. 4G).

Similarly, no differences were found between consecutive bones for all examined steps of DS (Fig. 5). However, the % of NP was higher in PIJ than TMJ for S1 (Fig. 6A) and higher in PIJ than DIJ for S4 (Fig. 6D), which indicate on the potential possibility of discrimination of narrow and wider tarsal joints not influenced by the type of normal TB.
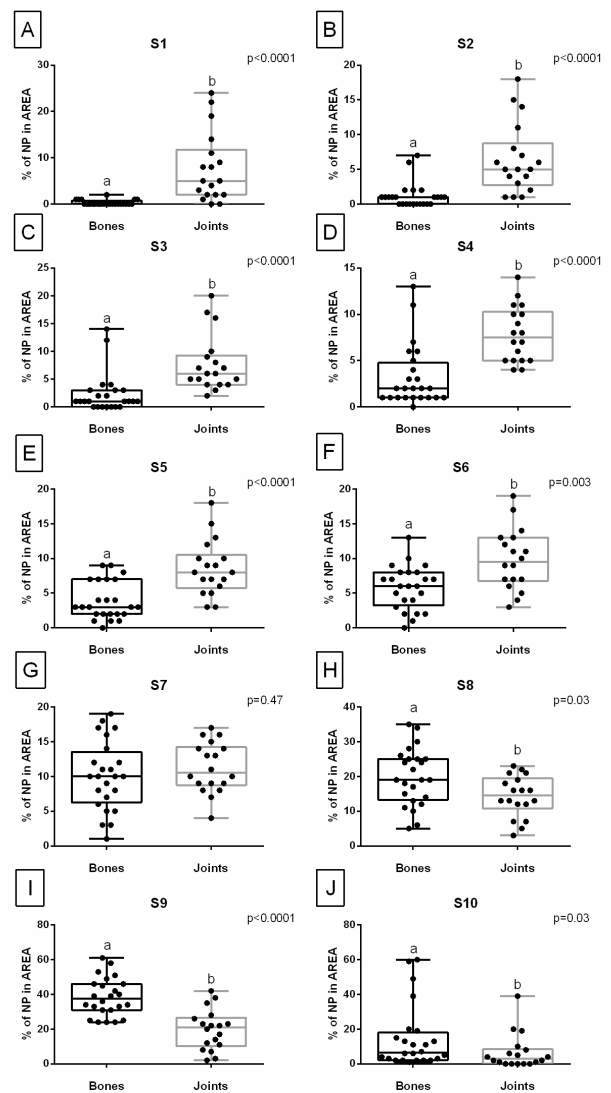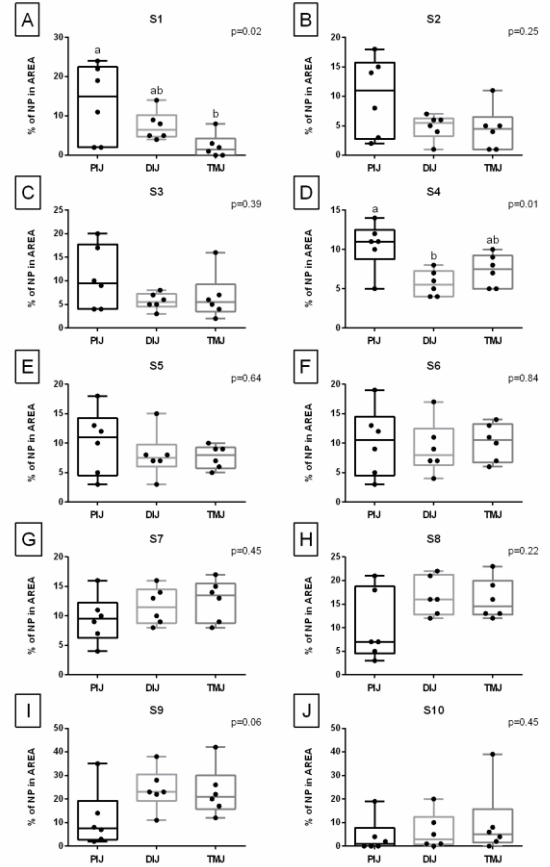

Fig. 4. The comparison of percentage (%) of the number of pixels (NP) in each AREA between all bones and joints anatomical structures. Data displayed separately for consecutive 10 steps (A, S1; B, S2; C, S3; D, S4; E, S5; F, S6; G, S7; H, S8; I, S9; J, S10) of density standard (DS). Data on box plots are represented by lower quartile, median and upper quartile, whereas whiskers represent minimum and maximum values. The single realisations are represented by dots. Lowercase letters indicate differences between groups for p < 0.05
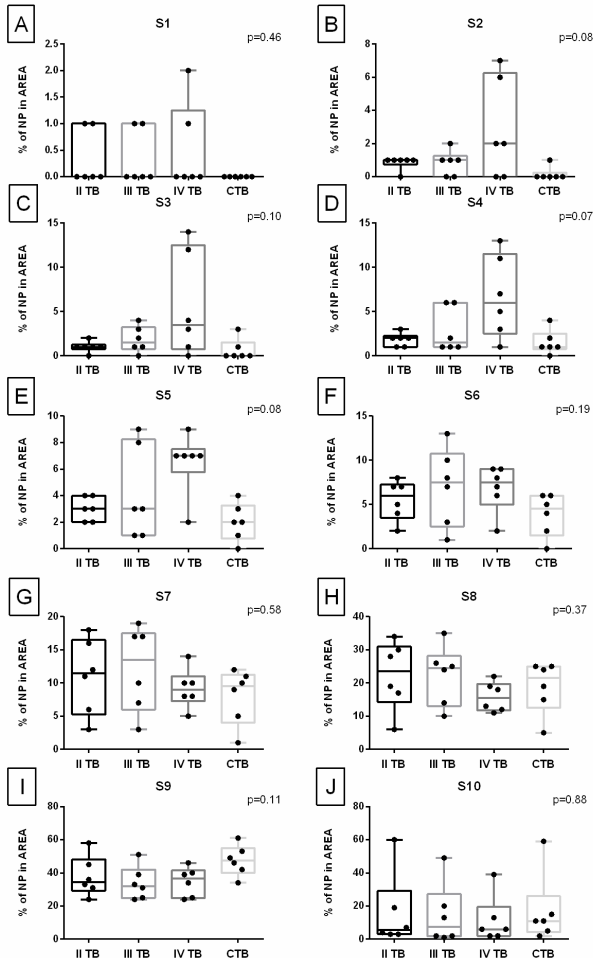
Fig. 5. The comparison of percentage (%) of the number of pixels (NP) in each AREA between consecutive bones' anatomical structures: II tarsal bone (II TB); III tarsal bone (III TB); IV tarsal bone (IV TB) and central tarsal bone (CTB). Data displayed separately for consecutive 10 steps (A, S1; B, S2; C, S3; D, S4; E, S5; F, S6; G, S7; H, S8; I, S9; J, S10) of density standard (DS). Data on box plots are represented by lower quartile, median and upper quartile, whereas whiskers represent minimum and maximum values. The single realisations are represented by dots. Lowercase letters indicate differences between groups for p < 0.05

4. DISCUSSION

Highlighting the most relevant results, one may observe that the application of this scaled–pixel–counting protocol allows quantification of the radiological features of joint spaces and bones and makes it possible to indicate the lucency of joint space and the opacity of bone structure. Thus, we confirm that the quantification of the radiological features of the anatomical structures of the equine normal tarsal joint is feasible. Knowing that the joint space narrowing, lysis of subchondral bone, sclerosis of subchondral bone, mineralisation front defects and osteophyte/enthesophyte development in OA-affected TB are the most important radiological signs [6, 7, 10, 11], the quantification of lucency and opacity may be considered as the first step for the tarsal joints rating. One may observe that on the radiographs, joint space narrowing is recognised as thin and uneven lucency between the adjacent cortical bones [6–9].

Fig. 6. The comparison of percentage (%) of the number of pixels (NP) in each AREA between consecutive joints' anatomical structures: proximal intertarsal joint (PIJ); distal intertarsal joint (DIJ) and tarsometatarsal joint (TMJ). Data displayed separately for consecutive 10 steps (A, S1; B, S2; C, S3; D, S4; E, S5; F, S6; G, S7; H, S8; I, S9; J, S10) of density standard (DS). Data on box plots are represented by lower quartile, median and upper quartile, whereas whiskers represent minimum and maximum values. The single realisations are represented by dots. Lowercase letters indicate differences between groups for p < 0.05

Therefore, in the case of OA when the lucency between bones is less than it should be, one can expect an increase in %NP of the bright steps (S7–S8) and a decrease in %NP of the dark steps (S1–S3) at the anatomical location of the joint spaces (PIJ, DIJ and/or TMJ ROIs).

This hypothesis needs to be tested in further studies using the OA-affected tarsal joints and comparing the results of the OA group with the results for normal joints presented in the current research. On the radiographs, lysis of the subchondral bone is recognised as the area of increased lucency within the cortical and subcortical bone [6–9]. Therefore, in the case of OA when the lucency within bones' anatomical locations is more than it should be, one can expect an increase in %NP of the dark steps (S1–S3) and a decrease in %NP of the bright steps (S8–S10) at the anatomical location of the bones (II TB, III TB, IV TB and/or CTB ROIs). On the radiographs, sclerosis of the subchondral bone is recognised as the area of increased opacity within the cortical and subcortical bones [6–9]. Therefore, in the case of OA when the opacity within bones' anatomical locations is more than it should be, one can expect an increase in %NP of the bright steps (S8–S10) and a decrease in %NP of the dark steps (S1–S3) at the

anatomical location of the bones (II TB, III TB, IV TB and/or CTB ROIs). On the radiographs, mineralisation front defects and osteophyte/enthesophyte development are recognised as the areas of increased opacity between the adjacent cortical bones [6–9]. Therefore, in the case of OA when the opacity between bones is more than it should be, one can expect an increase in %NP of the bright steps (S9–S10) and a decrease in %NP of the dark steps (S1–S3) at the anatomical location of the joint spaces (PIJ, DIJ and/or TMJ ROIs). The differentiation between the rating of joint space narrowing and mineralisation/osteophyte/enthesophyte should be assessed in detail since both radiological signs concern an increase in %NP of the bright steps and a decrease in %NP of the dark steps at the joint spaces. We suspect that estimation of bone density with HU will be helpful, with the advantage of %NP of S9–S10 in the case of new bone formations and %NP of S7–S8 in the case of narrowing. However, all these hypotheses need to be tested in further studies using the OA-affected tarsal joints and comparing the results of the OA group with the results for normal joints presented in the current research.

In the recent research, a radiographic rating scale, developed through the Delphi process, was employed for assessing OA radiographic signs in the tarsal joint. The rating was determined based on the total extent of the affected distal tarsal joint surface, leading to a qualitative verbal descriptive assessment of the

The four-point scale was used for the assessment of OA in the entire distal tarsus concerning none OA, mild OA, moderate OA and severe OA [18]. In the current research, a scaled–pixel–counting protocol was applied to all anatomical structures of the tarsal joint, resulting in a quantitative numerical rating of the normal joint. As no OA-affected joints were examined, the 4-point scale for the assessment of OA in the entire tarsal joint was not applied. Labens et al. [18] stated that if used clinically, this generalised assessment may not allow the progression of individual radiographic abnormalities to be monitored. Contrarily, the current scaled–pixel–counting protocol will be potentially able to distinguish the individual radiographic abnormalities since each bone and joint are quantified separately. However, all these hypotheses need to be tested in further studies using the OA-affected tarsal joints and comparing the results of the OA group with the results for normal joints presented in the current research.

In recent research, the basis of the radiographic rating scale was a visual analogue rating scale in which assessors indicated the severity of each radiographic feature as they perceived it [18]. In the current research, the basis of the radiographic rating protocol was the use of the DS and the automatic algorithm. In this protocol, assessors did not indicate the severity of each radiographic feature but only annotated the ROIs within the algorithm quantifying the relative values. The two-step relativisation, concerning the use of individual X-ray images of DS and the normalisation of NP values, makes the final results for each image as individual as possible. However, validation of the method on a larger set of valid and OA-affected data is necessary to continue the work that has been commenced in the current study.

5. CONCLUSION

An application of the scaled–pixel–counting protocol provides the quantitative radiological features of normal bone and joint structures of the tarsal joint in horses, making possible differentiation of the lucency of joint space and opacity of bone structure.

Moreover, the scaled–pixel–counting protocol allows for the discrimination of narrow and wider tarsal joints not influenced by the type of normal TB.

REFERENCES

1. Reed SA. Horses as athletes: the road to success. Animal Frontiers. 2022;12(3): 3-4.
https://doi.org/10.1093/af/vfac024
2. Baccarin RYA, Seidel SRT, Michelacci YM, Tokawa PKA, Oliveira TM. Osteoarthritis: a common disease that should be avoided in the athletic horse's life. Animal Frontiers. 2022;12(3):25-36.
https://doi.org/10.1093/af/vfac026
3. Latham CM, Guy CP, Wesolowski LT, White-Springer SH. Fueling equine performance: importance of mitochondrial phenotype in equine athletes. Animal Frontiers. 2022;12(3):6–14.
https://doi.org/10.1093/af/vfac023
4. Goodrich LR, Nixon AJ. Medical treatment of osteoarthritis in the horse–a review. The Veterinary Journal. 2006;171(1): 51-69.
https://doi.org/10.1016/j.tvjl.2004.07.008
5. De Sousa NR, Luna SP, Pizzigatti D, Martins MT, Possebon FS, Aguiar AC. Relation between type and local of orthopedic injuries with physical activity in horses. Ciência Rural. 2017;47: 1–7.
https://doi.org/10.1590/0103-8478cr20151218
6. Coppelman EB, David FH, Tóth F, Ernst NS, Trumble TN. The association between collagen and bone biomarkers and radiographic osteoarthritis in the distal tarsal joints of horses. Equine Veterinary Journal. 2020;52(3): 391-398.
https://doi.org/10.1111/evj.13187
7. Baxter GM, Southwood LL, Dechant JE. Diagnosis of distal tarsal osteoarthritis in horses. Compendium On Continuing Education For The Practising Veterinarian-North American Edition. 2003;25(2): 138–147.
8. Eksell P, Axelsson M, Broström H, Ronéus B, Häggström J, Carlsten J. Prevalence and risk factors of bone spavin in Icelandic horses in Sweden: a radiographic field study. Acta Veterinaria Scandinavica. 1998;39: 339-348.
https://doi.org/10.1186/BF03547782
9. Björnsdóttir S, Axelsson M, Eksell P, Sigurdsson H, Carlsten J. Radiographic and clinical survey of degenerative joint disease in the distal tarsal joints in Icelandic horses. Equine Veterinary Journal (2000);32(3): 268-272.
https://doi.org/10.2746/042516400776563590
10. Ley CJ, Björnsdóttir S, Ekman S, Boyde A, Hansson K. Detection of early osteoarthritis in the centrodistal joints of Icelandic horses: Evaluation of radiography and low-field magnetic resonance imaging. Equine Veterinary Journal. 2016;48(1): 57-64.
https://doi.org/10.1111/evj.12370
11. Fairburn A, Dyson S, Murray R. Clinical significance of osseous spurs on the dorsoproximal aspect of the third metatarsal bone. Equine Veterinary Journal. 2010;42: 591–599.
https://doi.org/10.1111/j.2042-3306.2010.00097.x
12. Dechant JE, Baxter GM, Southwood LL, et al. Use of a three-drilltract technique for arthrodesis of the distal tarsal joints in horses with distal tarsal osteoarthritis: 54 cases (1990–1999). Journal of the American Veterinary Medical Association. 2003;223(12): 1800–1805.
https://doi.org/10.2460/javma.2003.223.1800
13. Zubrod CJ, Schneider RK, Hague BA, Ragle CA, Gavin PR, Kawcak CE. Comparison of three methods for arthrodesis of the distal intertarsal and tarsometatarsal joints in horses. Veterinary Surgery. 2005;34: 372–382.
https://doi.org/10.1111/j.1532-950X.2005.00057.x
14. Gunther KP, Sun Y. Reliability of radiographic assessment in hip and knee osteoarthritis. Osteoarthritis Cartilage. 1999;7: 239–246.
https://doi.org/10.1053/joca.1998.0152

15. Kessler S, Dieppe P, Fuchs J, Sturmer T, Gunther KP. Assessing the prevalence of hand osteoarthritis in epidemiological studies. The reliability of a radiological hand scale. Annals of the Rheumatic Diseases. 2000;59: 289–292. doi: 10.1136/ard.59.4.289
Available from: https://ard.bmj.com/content/59/4/289

16. Innes JF, Costello M, Barr FJ, Rudorf H, Barr ARS. Radiographic progression of osteoarthritis of the canine stifle joint: a prospective study. Veterinary Radiology & Ultrasound. 2004;45(2): 143-148.
doi: 10.1111/j.1740-8261.2004.04024.x

17. Bjornsdottir S, Ekman S, Eksell P, Lord P. High detail radiography and histology of the centrodistal tarsal joint of Icelandic horses age 6 months to 6 years. Equine Veterinary Journal. 2004;36: 5–11.
https://doi.org/10.2746/0425164044864679

18. Labens R, Innocent GT, Voûte LC. Reliability of a quantitative rating scale for assessment of horses with distal tarsal osteoarthritis. Veterinary Radiology & Ultrasound. 2007;48(3): 204-211.
https://doi.org/10.1111/j.1740-8261.2007.00230.x

Marta Borowska: https://orcid.org/0000-0003-0148-9912

Bernard Turek: https://orcid.org/0000-0002-1065-5284

Paweł Lipowicz: https://orcid.org/0000-0003-3598-0945

Tomasz Jasiński: https://orcid.org/0000-0003-2906-9944

Katarzyna Skierbiszewska: https://orcid.org/0000-0002-1765-5340

Małgorzata Domino: https://orcid.org/0000-0001-9436-1074